UNIVERSITY OF BIRMINGHAM
University of Birmingham
Research at Birmingham

3-D printed slotted spherical resonator bandpass filters with spurious suppression
Zhang, Fan; Gao, Sufang; Li, Jin; Yu, Yang; Guo, Cheng; Li, Sheng; Attallah, Moataz; Shang, Xiaobang; Wang, Yi; Lancaster, Michael J.; Xu, Jun

Link to publication on Research at Birmingham portal

3-D Printed Slotted Spherical Resonator Bandpass Filters With Spurious Suppression

FAN ZHANG [ID] [1], **SUFANG GAO**[2], **JIN LI** [ID] [3], (Member, IEEE), **YANG YU** [ID] [4,5], **CHENG GUO** [ID] [4,6],
SHENG LI[7], **MOATAZ ATTALLAH**[7], **XIAOBANG SHANG** [ID] [8], (Senior Member, IEEE),
YI WANG [ID] [4], (Senior Member, IEEE), **MICHAEL J. LANCASTER** [ID] [4], (Senior Member, IEEE),
AND JUN XU[1]

[1] School of Physics, University of Electronic Science and Technology of China, Chengdu 610054, China
[2] Xi'an Microelectronics Technology Institute, Xi'an 710065, China
[3] Guangdong Provincial Mobile Terminal Microwave and Millimeter-Wave Antenna Engineering Research Center, College of Electronics and Information Engineering, Shenzhen University, Shenzhen 518060, China
[4] Department of Electronic, Electrical, and Systems Engineering, University of Birmingham, Birmingham B15 2TT, U.K.
[5] Department of Electrical and Electronics Engineering, Southern University of Science and Technology, Shenzhen 518055, China
[6] Department of Information and Communication Engineering, Xi'an Jiaotong University, Xi'an 710049, China
[7] School of Metallurgy and Materials, University of Birmingham, Birmingham B15 2TT, U.K.
[8] National Physical Laboratory, Teddington TW11 0LW, U.K.

Corresponding author: Sufang Gao (sufangg@yahoo.com)

ABSTRACT In this paper, a third-order waveguide bandpass filter (BPF) based on slotted spherical resonators with a wide spurious-free stopband is presented. The resonator consists of a spherical cavity with slots opened at the top and bottom. Compared with a non-slotted spherical resonator, the slotted resonator suppresses the two spurious modes (TM_{211} and TE_{101}) whilst maintaining the fundamental TM_{101} mode. The unloaded quality factor of the TM_{101} mode is not significantly degraded. This is achieved by interrupting surface current and radiating the unwanted spurious modes with the slots. The BPF is designed at a center frequency of 10 GHz with a fractional bandwidth of 1%. Two filter prototypes are fabricated, one using metal-based selective laser melting (SLM) and the other by polymer-based stereolithography apparatus (SLA) techniques. The slots also facilitate the copper electroplating process for the SLA-printed filter. The measured results show that the average passband insertion losses of the SLM- and SLA-printed filters are 0.33 and 0.2 dB, respectively. The corresponding passband return losses are better than 22 and 20 dB. The filters demonstrate excellent passband performance and wide spurious-free stopbands up to 16 GHz with stopband rejections of over 20 dB.

INDEX TERMS Bandpass filter, selective laser melting, slotted spherical resonator, spurious suppression, stereolithography apparatus, 3-D printing.

I. INTRODUCTION

Microwave resonators are the building blocks of passive microwave devices such as filters and multiplexers. Rectangular and cylindrical resonators [1]–[3] have been widely used because they can be readily fabricated using conventional manufacturing technologies. In recent years, additive manufacturing, also known as 3-D printing, has been reported in the fabrication of microwave devices. Complex geometries can be 3-D printed to enhance the performance of microwave

The associate editor coordinating the review of this article and approving it for publication was Xiu Yin Zhang.

devices [4]–[18]. A good example is the 3-D printed spherical resonator with intrinsically high unloaded quality factor (Q_u). In [4] and [5], spherical resonators were 3-D printed to construct waveguide bandpass filters (BPFs). The BPF in [4] exhibited a very low passband insertion loss (IL). However, the spherical resonator suffered from spurious modes spectrally close to the fundamental mode. This degraded the stopband performance of the filter. By using a 90°-twisted coupling geometry [4], the stopband rejection was improved because of the reduced coupling strength of the spurious TM_{211} mode. Another example is the mathematically defined super-ellipsoid resonators presented in [6] and [7] showing

excellent filtering performance. Other than that, there has been little work in spurious suppression for spherical resonator filters.

In this work, we focus on improving the spurious-free region of the spherical resonator BPFs. A new approach aiming to maximize the spurious suppression through slotting the cavities is presented. The spurious TM_{211} and TE_{101} modes of the spherical resonator are effectively suppressed without compromising the high Q_u of the fundamental TM_{101} mode. This significantly extends the spurious-free stopband. This is achieved by interrupting surface current of the spurious modes with slots. The slots are appropriately arranged on the cavity shells to ensure that the spurious TM_{211} and TE_{101} modes are suppressed and the fundamental TM_{101} mode is not disturbed. The principle of slotting differs from the work in [5] where a slot pattern was primarily used to facilitate the metallization process but not the spurious passband suppression. The proposed method of slotting in this work significantly enhances the spurious-free region. The method is potentially useful for other types of air-filled cavity resonators.

It should be noted that the proposed method does not represent a study of all possible slotted structures as there are far too many variables for simulations. Analytical solutions of this problem have not been attempted, and if possible to achieve, would be extremely complex. In the following, a third-order waveguide BPF based on slotted spherical resonators will be described. All the simulations were performed using Computer Simulation Technology (CST) Studio Suite [19].

II. SLOTTED SPHERICAL RESONATORS

Both the eigenmode simulation and the analytical formula in [20] show that the fundamental mode in a spherical resonator is TM_{101}. Here, it is worth making clear the designation of the mode index. To be consistent with [20] and the previous work in [4], for the TM_{nmp}/TE_{nmp} mode, n, m, and p denote r, φ, and θ in a spherical coordinate system, respectively, where r is the radial direction, φ is the azimuth angle (as indicated in Figs. 1 and 2 in relation to the spherical resonator), and θ is the elevation angle. There are a lot of degenerate higher order eigenmodes in a spherical resonator. The excitation of these modes depends on the feeding structure. When fed by a rectangular waveguide, the first two higher order modes are TM_{211} and TE_{101}. Shown in Fig. 1 are the simulated surface current distribution of the first four modes in a waveguide-fed spherical resonator. Fig. 1(a) shows the fundamental mode (TM_{101}) at 10 GHz with uniform current distribution along the φ direction (therefore $m = 0$). The resonant frequencies of the TM_{211} and TE_{101} modes are 14.08 and 16.39 GHz, respectively. These frequencies have been checked by calculations [20] and show good agreement. In order to suppress the spurious modes, a rectangular slot cutting into the spherical cavity, as illustrated in Fig. 2(a), is proposed. The suppression is realized by interrupting the surface current of the spurious modes so these modes radiate. As can be seen
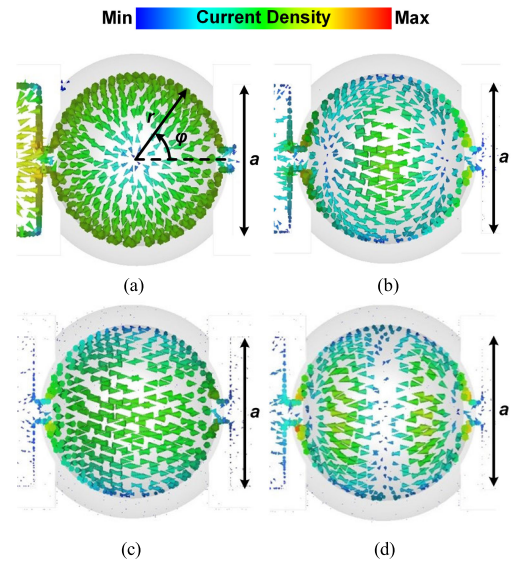

FIGURE 1. Simulated surface current distribution (top views) of the resonant modes in a two-port weakly coupled air-filled spherical resonator. (a) The TM_{101} mode. (b) The TM_{211} mode. (c) The TE_{101} mode. (d) The TM_{311} mode. The parameter a is the width of the feeding rectangular waveguide's broad wall.
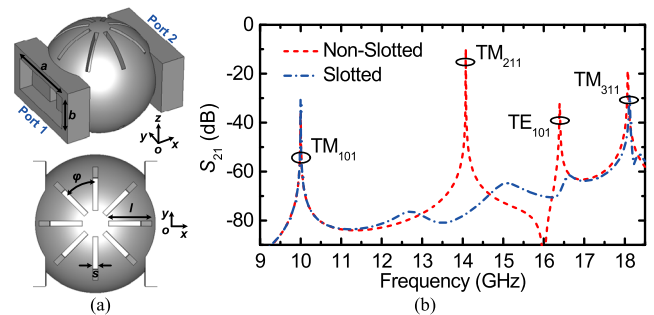

FIGURE 2. The slotted spherical resonator with weak waveguide external couplings. Feeding windows of 3.5 mm × 10.16 mm are used. (a) A structural illustration (upper: A 3-D view; lower: A top view). (b) EM-simulated transmission coefficient. Copper electrical conductivity of 5.96×10^7 S/m was used in the simulation for cavity boundaries. The slot dimensions are $s = 1.21$ mm, $l = 11.91$ mm, and $\varphi = 45°$.

from Fig. 1 and Fig. 2(a), the slots are parallel to the TM_{101}-mode surface current, but intersect the currents of the spurious modes. In addition, the slots are placed in a region with a low current density for the fundamental mode, but relatively large current densities for the spurious modes. Therefore, the TM_{211} and TE_{101} modes are suppressed through radiation without significantly interfering with the TM_{101} mode. This is verified by investigating the responses of the resonator model in Fig. 2(a). The simulated transmission coefficient (S_{21}) is plotted in Fig. 2(b). Note that, due to the existence of radiation, eigenmode simulation cannot be used. It is shown that the spurious resonances at 14.08 and 16.39 GHz have been effectively eliminated after the slots are introduced, whereas the TM_{101}-mode resonance is not affected. It should be mentioned that the spurious TM_{311} mode at 18.08 GHz has a similar current distribution as the TM_{101} mode, as shown in Fig. 1(d). So suppression of the TM_{311} mode and others beyond without affecting the TM_{101} mode can be difficult.
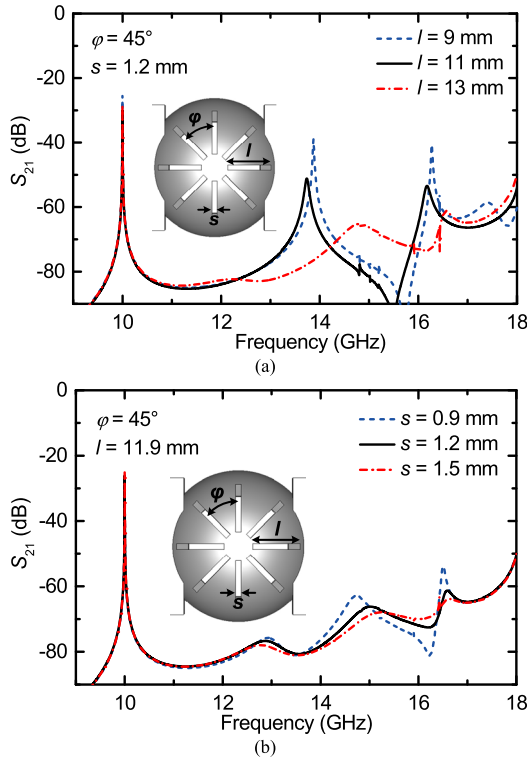
FIGURE 3. EM-simulated transmission responses of the slotted spherical resonator with different slot dimensions. (a) The wideband transmission coefficient versus slot length *l*. (b) The wideband transmission coefficient versus slot width *s*.

It is worth mentioning that another well-known technique for spurious mode suppression is to look for coupling geometries which couple to the fundamental mode but not the spurious. However, in this case we have not found a more effective way than the proposed approach by slotting.

EM-simulated transmission responses of the slotted spherical resonator under different slot dimensions are graphically compared in Fig. 3. The results show that the suppression level is mainly determined by the slot length *l*. As the length *l* is increased from 9 to 13 mm, the suppression of the TM_{211} and TE_{101} modes is significantly enhanced, as shown in Fig. 3(a). This is because in the slotted region the current for the spurious modes is concentrated and longer slots interrupt the current more effectively. The suppression level is also affected by the slot width *s*, as shown in Fig. 3(b), but in a much less significant way.

It is important to quantify the influences of the slots on the TM_{101}-mode resonance. This is accomplished by simulations as follows. The loaded quality factor (Q_L) and unloaded quality factor (Q_u) of the slotted spherical resonator in free space can be expressed as [21]

$$Q_L^{-1} = Q_e^{-1} + Q_c^{-1} + Q_r^{-1}, \qquad (1)$$
$$Q_u^{-1} = Q_c^{-1} + Q_r^{-1}. \qquad (2)$$

Here Q_e is the external quality factor associated with the coupling aperture between the feeding rectangular waveguide and the resonator. Q_r and Q_c are the radiation quality factor and conductor quality factor, respectively. We are interested

in finding Q_r due to the slots for the TM_{101} mode and comparing it with Q_c. The calculation of the quality factors of the slotted spherical resonator, with $s = 1.21$ mm and $l = 11.91$ mm, is exemplified as follows. Firstly, to find Q_e we use an unslotted spherical resonator with the coupling aperture set to be 2.5 mm by 10.16 mm. We make the material a perfect electrical conductor (PEC), hence there is no radiation loss or conductor loss. From (1) this gives $Q_L = Q_e$, which by simulation turns out to be 1.67×10^7. Now the slotted resonator is also simulated with PEC, resulting in a value of $Q_L = 1.5 \times 10^6$. From (1) and the previously calculated Q_e, the value of Q_r can be calculated as 1.64×10^6. Next, the material is changed from PEC to copper with an electrical conductivity of 5.96×10^7 S/m. The simulation of the slotted resonator produces a Q_L of 1.42×10^4. Knowing the values of Q_L, Q_e, and Q_r in equation (1) allows the calculation of Q_c, which becomes $Q_c = 1.43 \times 10^4$. Since Q_e and Q_r are at least two orders of magnitude larger than Q_c, they have very little influence on Q_L in this case. It should be noted that this calculation is only an approximation, but it is good because of the large differences in the Q values. This allows us to conclude that Q_r has virtually no influence on the TM_{101} mode as $Q_c \ll Q_r$. Using the calculated Q_c and Q_r, the Q_u value of the slotted spherical resonator is obtained from (2) as 1.42×10^4. This value is very close to the Q_u (1.44×10^4) of a non-slotted spherical resonator.

Using the above-mentioned method, TM_{101}-mode quality factors of the slotted spherical resonator under different slot dimensions are calculated and plotted in Fig. 4. The simulated result shows that increasing *s* or *l* only reduces Q_c and Q_u by
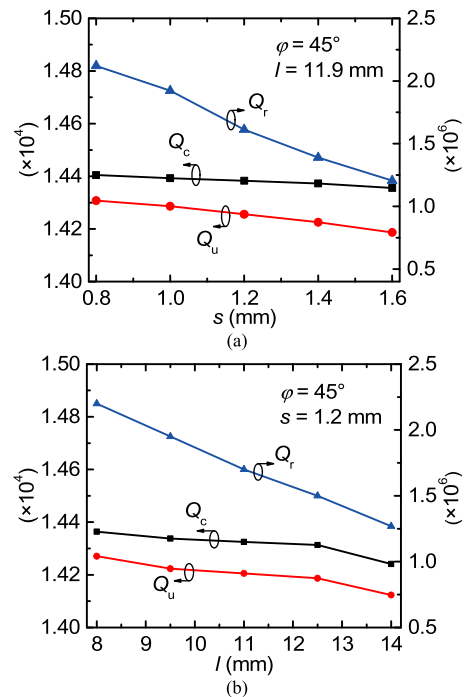

FIGURE 4. Simulated TM_{101}-mode quality factors of a slotted spherical resonator under different slot dimensions. (a) The quality factors versus slot width *s*. (b) The quality factors versus slot length *l*.
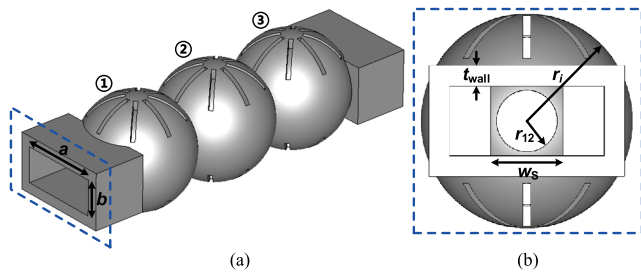
FIGURE 5. A geometrical illustration of the third-order *X*-band BPF based on the slotted spherical resonators. (a) A 3-D view. (b) A side view ($i = 1$, 2, and 3 for the radius r_i of the ith resonator, respectively).

TABLE 1. Critical dimensions of the designed *X*-Band BPF (Units: mm).

a	b	w_S	r_{12}	r_{23}	r_1	r_2	r_3	t_{wall}	s	l
22.86	10.16	10.73	4.56	4.56	12.71	12.89	12.71	3	1.21	11.79

less than 1.5% over the inspected region of the dimensions. This shows that negligible conductor loss is introduced from the enlarged slots. In contrast, Q_r decreases by over 40%. However, it is still much higher than Q_c ($\sim 10^4$), indicating very little radiation loss for the TM_{101} mode. From (2), it is known that the degraded but large Q_r has little effect on Q_u. The choice of the slots sizes has been a good balance between the suppression level of the higher modes and Q_u of the fundamental mode.

III. SLOTTED SPHERICAL RESONATOR FILTER DESIGN

To validate the spurious passband suppression for BPFs using the proposed slotted spherical resonators, a third-order waveguide filter was designed. The constituent slotted spherical resonators of the filter were configured with an inline coupling geometry as illustrated in Fig. 5(a). The filter was designed with a Chebyshev transfer function with a center frequency (f_0) of 10 GHz, a fractional bandwidth (FBW) of 1%, and a passband return loss (RL) of 20 dB. The coupling matrix methodology was used [21]. The external quality factor (Q_e) and denormalized inter-resonator coupling coefficients were calculated to be $Q_e = 85.1$ and $K_{12} = K_{23} = 0.0103$. In the practical filter, Q_e is controlled by the width w_S of the rectangular coupling apertures at the source and load. The inter-resonator coupling coefficients K_{12} and K_{23} are controlled by the radii r_{12} and r_{23}, respectively, as labeled in Fig. 5(b). The extracted Q_e and inter-resonator coupling coefficients as a function of the dimensions are plotted in Fig. 6. The coupling strength is enhanced with the increase of r_{12} and r_{23}, and the external coupling becomes stronger (smaller Q_e) as w_S increases. The required design parameters can be obtained from Fig. 6 and the final dimensions of the filter is summarized in Table 1. The simulated transmission response of the filter is presented in Fig. 7 in comparison with that of a reference filter with non-slotted spherical resonators of the same design specifications. It is shown that the spurious passbands of the slotted resonator filter at around 14 and 16.5 GHz are suppressed and the spurious-free stopband is greatly extended.
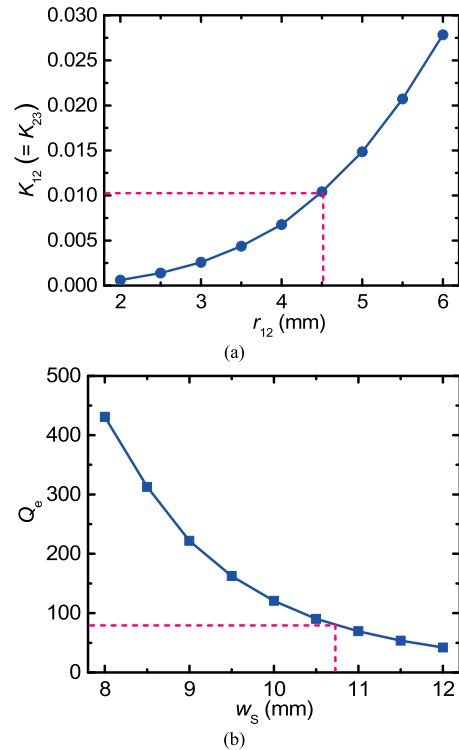

FIGURE 6. Extracted $K_{12} (= K_{23})$ and Q_e values from EM simulation. (a) $K_{12} (= K_{23})$ versus r_{12}. (b) Q_e versus w_S. The pink dash lines point out the required design parameters.
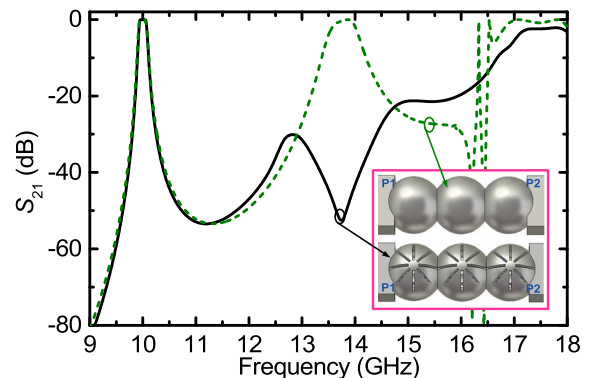

FIGURE 7. EM-simulated wideband transmission responses of the BPFs. P1 and P2 stand for ports 1 and 2.

IV. FILTER FABRICATION

It would be very difficult to make the filter by conventional means due to the complex geometry. Therefore, additive manufacturing technology was used. To demonstrate the capability of 3-D printing, both the metallic selective laser melting (SLM) and the polymer-based stereolithography apparatus (SLA) were used to produce two filter prototypes.

The benefits and drawbacks of the SLM and SLA processes are different. For SLM, the fabricated components have higher mechanical robustness but with heavier weight and may need a subsequent polishing process to reduce the surface roughness. For SLA, the constructed devices have lighter weight and generally higher dimensional accuracy but need a surface metallization process [18].
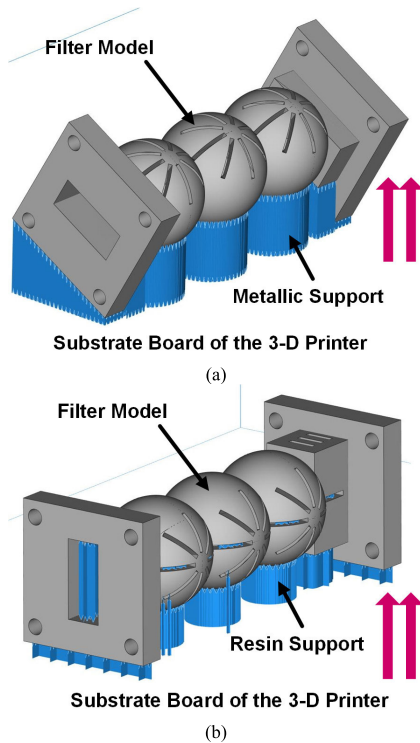
FIGURE 8. Illustrations of the orientations of the BPF models under 3-D printing, (a) for SLM printing and (b) for SLA printing. The red arrows indicate the printing direction.

The first prototype was SLM-printed with an aluminum-copper-based alloy (92 weight percent (wt. %) aluminum, 5 wt. % copper, and 3 wt. % others) in a powder form supplied in 15–53-μm particle size. The alloy was chosen due to its availability as a standard 3-D printing material, as opposed to other aluminum alloys that are not normally used [22]. A printing orientation, as illustrated in Fig. 8(a), was selected to ensure that no metallic support is required inside the cavities. Any internal metallic support would be very difficult to remove. After the printing process was completed, the metallic support structure outside the filter was removed manually.

The second prototype was SLA-printed with an Accura Xtreme resin [23] with a printing resolution of 50 μm. The orientation for the printing is illustrated in Fig. 8(b). For SLA, it is generally easier to remove resin support, so that the orientation can be selected more flexibly. There was no internal support after the filter model was printed and cleaned. After the resin curing process, 10-μm thick copper was plated onto the printed resin using the same process as in [4] and [5]. This thickness of copper was subtracted from the filter model before the 3-D printing by performing a structural compensation. This minimizes any frequency shift of the fabricated filter. It is very important to note that the slots on the spherical resonators are also used to facilitate the metal coating process. It can be seen from Fig. 8(b) that additional slots are cut in the input and output waveguide sections for the same purpose.

V. MEASUREMENT AND DISCUSSION

The 3-D printed filters were measured using a Keysight E8362C network analyzer under a two-port waveguide thru-reflect-line calibration. The frequency responses at *X* and *Ku* bands were measured separately. For the *Ku*-band measurement, a pair of *X*-to-*Ku*-band waveguide tapers were used, and the network analyzer was calibrated at *Ku* band. The EM-simulated and measured frequency responses of the SLM-printed filter are compared in Fig. 9, showing good agreement. The average measured passband IL is about 0.62 dB and the RL is greater than 22 dB. The IL is 0.4–0.5 dB higher than the simulated value. Assuming this IL increment is solely attributed to the surface roughness of the printed alloy, it corresponds to an equivalent root mean square roughness (R_q) of about 2.5 μm. It is not straightforward to measure the surface roughness as the resonators are enclosed. In addition, the roughness varies depending upon the deposition angle and is not uniform. The figure of 2.5 μm is not an unreasonable average. There is more discussion of this below for the polished filter. The re-simulated S_{21} parameter taking into account the 2.5-μm surface roughness agrees better with the measured one, as shown in Fig. 9(a). The measured Q_u for the slotted spherical resonator is estimated to be 2830 [21]. The measured frequency shift (Δf) is about 0.5% and is caused by volume shrinkage of the metal-printed cavities. Shrinkage is usually induced during the laser melting process because of the phase transformation and the contraction of solids when cooled from the solidification temperature to ambient temperature [24]. The shrinkage caused a small error in the size which could be minimized by a structural compensation before the printing.

To further reduce the passband IL, a vibration grinding process was performed on the metal-printed filter. The fabricated filter was immersed in the vibration grinding machine tank filled with water and abrasive materials, as shown in Fig. 10(a). The inner and outer surfaces of the filter were polished. This improved the effective electrical conductivity of the 3-D printed aluminum alloy and thus decreased the associated conductor loss. The control of the polishing time was very important. Experiments showed that when the structure was ground for too long, the improvement in the surface finish would not be as significant as at the beginning. Even worse, some critical geometries may be worn out, deteriorating the filter's RF performance. In this work, the filter was measured after 2 and 8 hours of polishing. The measured passband responses are plotted in Fig. 10(b) and compared with the measurement before the polishing. As can be seen, the measured passband IL of the filter is decreased with the increasing time of polishing. After 2 hours, the passband IL is reduced to around 0.5 dB. The IL is further reduced to around 0.33 dB after 8 hours, approaching the simulated IL value of 0.25 dB. Assuming all the loss is due to the roughness, the corresponding equivalent R_q is improved to 1 μm. The measured Q_u of the slotted spherical resonator is improved to 4060, about 43% higher than the value before the polishing.
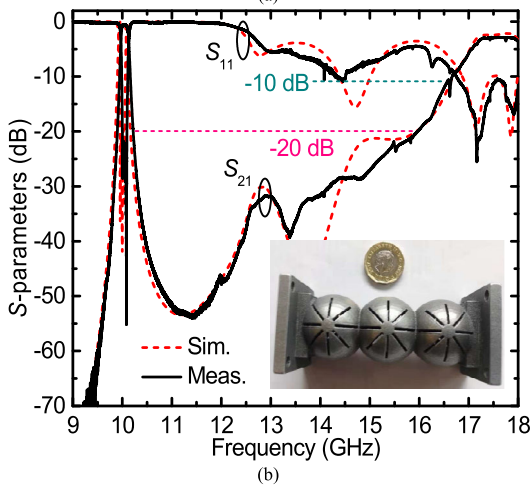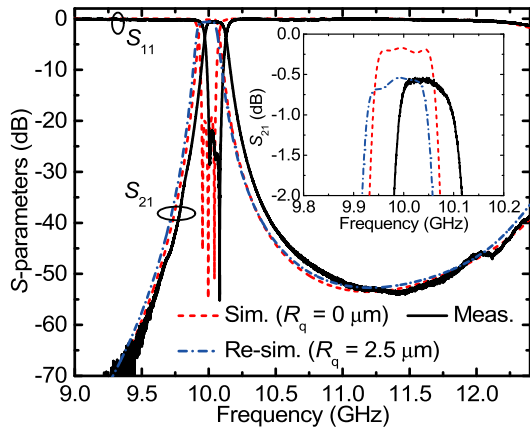
FIGURE 9. The SLM-printed filter. (a) EM-simulated and RF-measured passband responses. (b) Wideband responses. The inset shows a photograph of the filter.

FIGURE 10. The surface polishing process for the metallic SLM-printed filter. (a) Photograph of the vibration grinding machine. The grey particles are abrasive materials. (b) Passband responses of the filter before and after the polishing process.
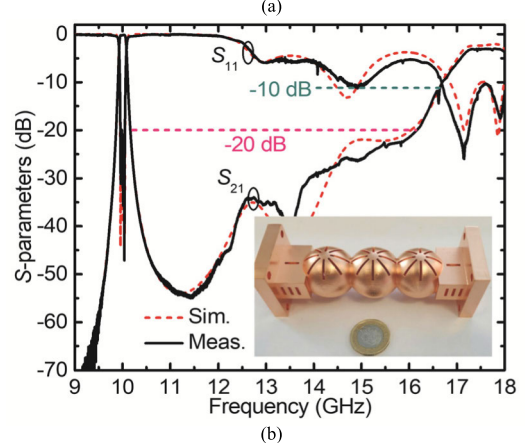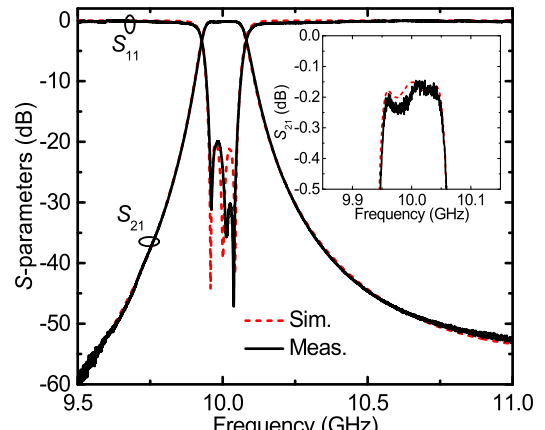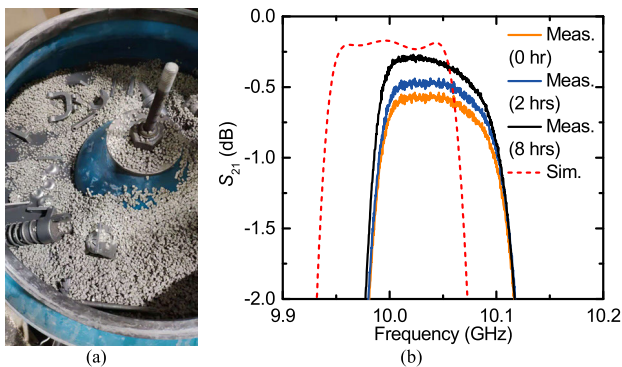

FIGURE 11. The SLA-printed filter. (a) EM-simulated and RF-measured passband responses. (b) EM-simulated and RF-measured wideband responses. The inset shows a photograph of the filter.

The measured reflection response before and after polishing shows little difference.

For the second prototype based on SLA, the EM-simulated and RF-measured frequency responses are compared in Fig. 11, showing much better agreement in terms of the

passband IL and a negligible frequency shift, as compared with the metal 3-D printed prototype. In the passband, the measured average IL and minimum RL are 0.2 and 20 dB, respectively. The measured IL is only 0.05 dB higher than the simulated one. The measured Δf is as small as 0.04% (4 MHz), indicating accurate reproduction of the structure. Noteworthy is that shrinkage also occurs in SLA process and can be induced by phase transformation of the resin from liquid to solid [25]. However, it is much less prominent because no high temperature is involved in the SLA process. As can be seen from Figs. 9(b) and 11(b), both filter prototypes demonstrate wide spurious-free stopbands with rejections over 20 dB up to 16.2 GHz, with the spurious passbands at around 14 and 16.5 GHz suppressed. The first spurious passband appears beyond 17 GHz. Photographs of the fabricated filters are included in the insets of Figs. 9(b) and 11(b).

Fig. 12 shows the loss factor in the filters calculated using $1 - |S_{11}|^2 - |S_{21}|^2$. This provides information on losses due to the metal as well as the radiation. It can be seen that at the higher spurious mode frequencies the loss is very high due to the enhanced radiation. Within the passband, the loss is mainly caused by the effective conductor loss, and the loss (~ 0.2 dB) in the SLA-printed filter is smaller than the
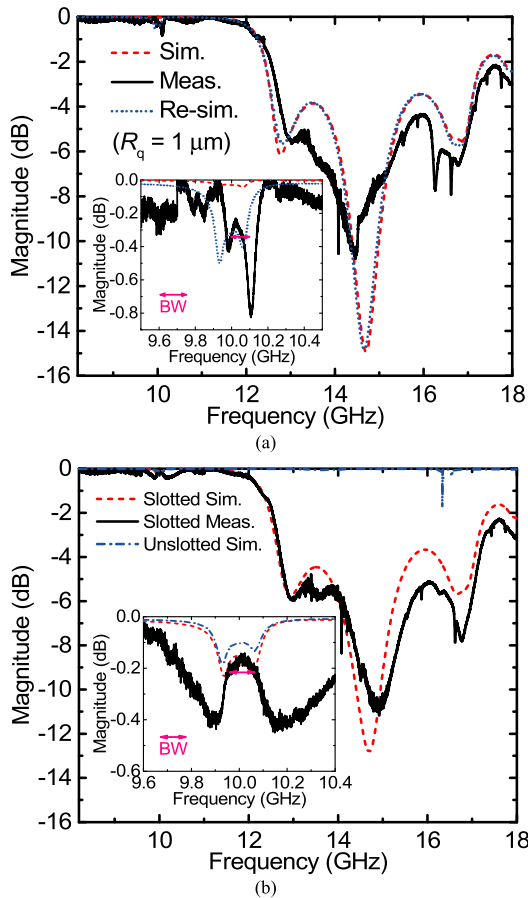
FIGURE 12. EM-simulated and RF-measured loss factors ($1-|S_{11}|^2 - |S_{21}|^2$) of the filters. (a) The SLM-printed filter. (b) The SLA-printed filter.

TABLE 2. Comparison with previously reported 3-D Printed BPFs.

Ref.	Res.	f_0 (GHz)	FBW (%)	IL (dB)	RL (dB)	Δf (%)	Spurious Suppression	f_1/f_0
[4]	S	10	5	0.11	>20	0.05	—	1.32:1
[5]	SS	10	3	0.24	>18	<0.01	—	1.27:1
[6]	SE	12.875/ 14.125	1.94/ 1.77	0.2	>18	<0.2	Yes (>55 dB)	>1.7:1
[8]	H	32	1/5	0.43–1	>10–17	<0.47	—	1.37:1
[9]	SS	10	3	0.24	>17	0.8	—	1.27:1
[10]	R	87.5	11.5	0.3–0.5	>18	2.78	—	—
T.W.	SS	10	1	0.2	>20	0.04	Yes (>20 dB)	>1.7:1
T.W.	SS	10	1	0.33	>22	0.5	Yes (>20 dB)	>1.7:1

*T.W.: This work; Res.: Resonators; S: Spherical; SS: Slotted spherical; H: Hemispherical; SE: Super-ellipsoid; R: Rectangular; f_1/f_0: Frequency ratio of the first spurious passband to the fundamental-mode passband.

loss in the SLM-printed filter (0.23–0.7 dB). This indicates a higher electrical conductivity and lower surface roughness of the plated copper than that of the aluminum alloy. Furthermore, within the passband the simulated loss difference between the non-slotted and slotted filters is less than 0.05 dB from Fig. 12(b), validating the negligible passband radiation. The impact of stopband radiation to external circuits can be mitigated by attaching microwave absorbers to the slots.

The measured results of the filters with the absorbers show no significant difference to the ones in Figs. 9 and 11 in terms of the passband and the stopband responses. Finally, a comparison of the proposed filters to previous related work is summarized in Table 2. The filters reported here exhibit extended spurious-free stopbands compared to previous filters in [4], [5], [8], and [9]. The proposed method of slotting can be extrapolated to higher order filters with flexible slot patterns to further enhance the stopband performance.

VI. CONCLUSION
A high-Q slotted spherical resonator is proposed to suppress spurious passbands of spherical resonator based bandpass filters. The spurious TM_{211} and TE_{101} modes are eliminated, and an extended spurious-free stopband ($f_1/f_0 > 1.7:1$) is realized without significantly compromising the performance of the fundamental-mode passband. The filters made by two 3-D printing techniques, i.e., SLM and SLA, demonstrate good process quality and flexibility. The excellent passband performance of the fabricated filters validates the capability of the utilized 3-D printing process for microwave waveguide devices.

REFERENCES
[1] G. F. Craven and C. K. Mok, "The design of evanescent mode waveguide bandpass filters for a prescribed insertion loss characteristic," *IEEE Trans. Microw. Theory Techn*, vol. MTT-19, no. 3, pp. 295–308, Mar. 1971.

[2] S. Amari, "Application of representation theory to dual-mode microwave bandpass filters," *IEEE Trans. Microw. Theory Techn.*, vol. 57, no. 2, pp. 430–441, Feb. 2009.

[3] R. J. Cameron and J. D. Rhodes, "Asymmetric realizations for dual-mode bandpass filters," *IEEE Trans. Microw. Theory Techn.*, vol. MTT-29, no. 1, pp. 51–58, Jan. 1981.

[4] C. Guo, X. Shang, M. J. Lancaster, and J. Xu, "A 3-D printed lightweight X-band waveguide filter based on spherical resonators," *IEEE Microw. Wireless Compon. Lett.*, vol. 25, no. 7, pp. 442–444, Jul. 2015.

[5] C. Guo, X. Shang, J. Li, F. Zhang, M. J. Lancaster, and J. Xu, "A lightweight 3-D printed X-band bandpass filter based on spherical dual-mode resonators," *IEEE Microw. Wireless Compon. Lett.*, vol. 26, no. 8, pp. 568–570, Aug. 2016.

[6] P. Booth and E. V. Lluch, "Enhancing the performance of waveguide filters using additive manufacturing," *Proc. IEEE*, vol. 105, no. 4, pp. 613–619, Apr. 2017.

[7] P. A. Booth and E. V. Lluch, "Realising advanced waveguide bandpass filters using additive manufacturing," *IET Microw., Antennas Propag.*, vol. 11, no. 14, pp. 1943–1948, Nov. 2017.

[8] J. Li, C. Guo, L. Mao, J. Xiang, G.-L. Huang, and T. Yuan, "Monolithically 3-D printed hemispherical resonator waveguide filters with improved out-of-band rejections," *IEEE Access*, vol. 6, pp. 57030–57048, 2018.

[9] C. Guo, J. Li, D. D. Dinh, X. Shang, M. J. Lancaster, and J. Xu, "Ceramic filled resin based 3D printed X-band dual-mode bandpass filter with enhanced thermal handling capability," *Electron. Lett.*, vol. 52, no. 23, pp. 1929–1931, Nov. 2016.

[10] X. Shang, P. Penchev, C. Guo, M. J. Lancaster, S. Dimov, Y. Dong, M. Favre, M. Billod, and E. de Rijk, "W-band waveguide filters fabricated by laser micromachining and 3-D printing," *IEEE Trans. Microw. Theory Techn.*, vol. 64, no. 8, pp. 2572–2580, Aug. 2016.

[11] A. I. Dimitriadis, T. Debogovic, M. Favre, M. Billod, L. Barloggio, J.-P. Ansermet, and E. de Rijk, "Polymer-based additive manufacturing of high-performance waveguide and antenna components," *Proc. IEEE*, vol. 105, no. 4, pp. 668–676, Apr. 2017.

[12] O. A. Peverini, G. Addamo, R. Tascone, G. Virone, P. Cecchini, R. Mizzoni, F. Calignano, E. P. Ambrosio, D. Manfredi, and P. Fino, "Enhanced topology of E-plane resonators for high-power satellite applications," *IEEE Trans. Microw. Theory Techn.*, vol. 63, no. 10, pp. 3361–3373, Oct. 2015.

[13] O. A. Peverini, G. Addamo, M. Lumia, G. Virone, F. Calignano, M. Lorusso, and D. Manfredi, "Additive manufacturing of Ku/K-band waveguide filters: A comparative analysis among selective-laser melting and stereo-lithography," *IET Microw., Antennas Propag.*, vol. 11, no. 14, pp. 1936–1942, Nov. 2017.

[14] G.-L. Huang, C.-Z. Han, W. Xu, T. Yuan, and X. Zhang, "A compact 16-way high-power combiner implemented via 3-D metal printing technique for advanced radio-frequency electronics system applications," *IEEE Trans. Ind. Electron.*, vol. 66, no. 6, pp. 4767–4776, Jun. 2019.

[15] G.-L. Huang, S.-G. Zhou, C.-Y.-D. Sim, T.-H. Chio, and T. Yuan, "Lightweight perforated waveguide structure realized by 3-D printing for RF applications," *IEEE Trans. Antennas Propag.*, vol. 65, no. 8, pp. 3897–3904, Aug. 2017.

[16] G. Addamo, O. A. Peverini, D. Manfredi, F. Calignano, F. Paonessa, G. Virone, R. Tascone, and G. Dassano, "Additive manufacturing of Ka-band dual-polarization waveguide components," *IEEE Trans. Microw. Theory Techn.*, vol. 66, no. 8, pp. 3589–3596, Aug. 2018.

[17] O. A. Peverini, M. Lumia, G. Addamo, F. Paonessa, G. Virone, R. Tascone, F. Calignano, G. Cattano, and D. Manfredi, "Integration of an *H*-plane bend, a twist, and a filter in Ku/K-band through additive manufacturing," *IEEE Trans. Microw. Theory Techn.*, vol. 66, no. 5, pp. 2210–2219, May 2018.

[18] G. Venanzoni, M. Dionigi, C. Tomassoni, and R. Sorrentino, "3-D-printed quasi-elliptical evanescent mode filter using mixed electromagnetic coupling," *IEEE Microw. Wireless Compon. Lett.*, vol. 28, no. 6, pp. 497–499, Jun. 2018.

[19] AG, USA. (Jul. 2018). *CST Computer Simulation Technology*. [Online]. Available: https://www.cst.com

[20] K. Zhang and D. Li, *Electromagnetic Theory for Microwaves and Opto-electronics*. Berlin, Germany: Springer-Verlag, 2008.

[21] J. S. Hong and M. J. Lancaster, *Microstrip Filters for RF/Microwave Applications*. New York, NY, USA: Wiley, 2001.

[22] I. Gibson, D. Rosen, and B. Stucker, *Additive Manufacturing Technologies: Rapid Prototyping to Direct Digital Manufacturing*. Berlin, Germany: Springer-Verlag, 2010.

[23] 3D Systems, Inc. (Sep. 2018). *Accura Xtreme*. [Online]. Available: www.3dsystems.com

[24] H. H. Zhu, L. Lu, and J. Y. Fuh, "Study on shrinkage behaviour of direct laser sintering metallic powder," *Proc. Inst. Mech. Eng. B, J. Eng. Manuf.*, vol. 220, no. 2, pp. 183–190, Feb. 2006.

[25] W. L. Wang, C. M. Cheah, J. Y. H. Fuh, and L. Lu, "Influence of process parameters on stereolithography part shrinkage," *Mater. Des.*, vol. 17, no. 4, pp. 205–213, 1996.
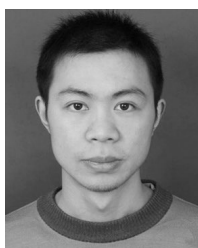
FAN ZHANG was born in Sichuan, China. He is currently pursuing the Ph.D. degree in radio physics with the School of Physics, University of Electronic Science and Technology of China, Chengdu, China.

From 2017 to 2018, he was a Visiting Student with the University of Birmingham, Birmingham, U.K. His current research interests include the design of microwave filters, 3-D printed filters, tunable filters, and millimeter-wave circuits.

SUFANG GAO was born in Shaanxi, China, in 1976. She received the B.E. degree in mechanical design and manufacturing of electromechanical engineering from North University, Taiyuan, China, in 2000, and the M.S. degree in circuits and systems from Northwest University, Xi'an, China, in 2005.

From 2016 to 2017, she was an Academic Visitor with the University of Birmingham, Birmingham, U.K. Since 2014, she has been a Professor in hybrid integrated circuits design with Xi'an Microelectronics Technology Institute, Xi'an. Her research interests include the design of microwave circuits and transceiver modules.

JIN LI (S'11–M'17) received the B.E. degree in electronic information engineering and the Ph.D. degree in radio physics from the University of Electronic Science and Technology of China, Chengdu, China, in 2010 and 2017, respectively.

He was a Visiting Research Scholar with the Birck Nanotechnology Center, School of Electrical and Computer Engineering, Purdue University, West Lafayette, IN, USA, from 2013 to 2015, supported by the China Scholarship Council through the State Scholarship Fund. He was an External Research Specialist with the ATR National Key Laboratory of Defense Technology, Shenzhen University, Shenzhen, China, from 2017 to 2018. He is currently a Postdoctoral Research Fellow of the College of Electronics and Information Engineering, Shenzhen University. His current research interests include RF design and characterization of reconfigurable microwave filters, microwave passive devices, RF microelectromechanical systems, thin film materials, and in addition manufactured RF components.

Dr. Li is a member of the IEEE Microwave Theory and Techniques Society (IEEE MTT-S), the Chinese Institute of Electronics, and the Applied Computational Electromagnetics Society (ACES). He is the co-recipient of the First Place Award from the 2014 and 2015 IEEE MTT-S International Microwave Symposium Tunable RF-MEMS Filter Student Design Competition. He is a Reviewer of several IEEE/IET/Wiley/ACES journals and international conferences.

YANG YU was born in Tianjin, China, in 1991. He received the B.E. degree in communication engineering and the M.E. degree in information and communication engineering from Tianjin Polytechnic University, Tianjin, in 2013 and 2016, respectively. He is currently pursuing the Ph.D. degree with the University of Birmingham, Birmingham, U.K., and the Southern University of Science and Technology, Shenzhen, China.

His current research interests include synthesis and design of RF/microwave components and computational intelligence techniques for engineering.

CHENG GUO was born in Chengdu, China, in 1990. He received the B.E. degree in communication engineering from Southwest Jiaotong University (Emei), Chengdu, in 2012, and the Ph.D. degree in radio physics from the University of Electronic Science and Technology of China, Chengdu, in 2016.

From 2014 to 2016, he was a Visiting Ph.D. Student with the University of Birmingham, Birmingham, U.K., where he was a Research Fellow, from 2017 to 2018. He is currently an Associate Professor with the Department of Information and Communication Engineering, Xi'an Jiaotong University, Xi'an, China. His current research interests include 3-D printed passive microwave devices, Schottky diode-based THz frequency multipliers and mixers, and micromachined millimeter-wave/THz circuits.

Dr. Guo is the co-recipient of the Tatsuo Itoh Award from the IEEE Microwave Theory and Techniques Society, in 2017.

F. Zhang *et al.*: 3-D Printed Slotted Spherical Resonator BPFs With Spurious Suppression
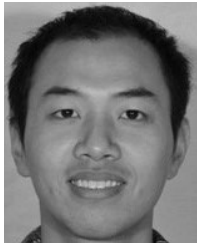
SHENG LI was born in Guangzhou, China, in 1988. He received the B.S. degree in materials science from the Wuhan University of Science and Technology, Wuhan, China, in 2011, and the Ph.D. degree in materials science from the University of Birmingham, Birmingham, U.K., in 2016.

From 2016 to 2018, he was a Research Fellow with the School of Metallurgy and Materials, University of Birmingham, where he has been a Research Fellow with the Department of Mechanical Engineering, since 2018.

MOATAZ ATTALLAH received the Ph.D. degree from the University of Birmingham, Birmingham, U.K., in 2007.

Since 2007, he has been a Research Scientist with the University of Manchester, U.K., prior to his appointment in Birmingham, in 2010. He is currently a Professor of advanced materials processing with the School of Metallurgy and Materials, University of Birmingham. He has established a large research group that investigates a number of advanced manufacturing processes, one of which is metal 3-D printing. He has collaborated with key companies in aerospace, space, medical, defense, and energy sectors in U.K., Europe, Japan, and China. He is the Co-inventor of seven patent applications. He has coauthored over 100 journals and conference articles and two book chapters.

XIAOBANG SHANG (M'13–SM'19) was born in Hubei, China, in 1986. He received the B.E. degree (Hons.) in electronic and communication engineering from the University of Birmingham, Birmingham, U.K., in 2008, the B.E. degree in electronics and information engineering from the Huazhong University of Science and Technology, Wuhan, China, in 2008, and the Ph.D. degree in microwave engineering from the University of Birmingham, in 2011. His doctoral research concerned with micromachined terahertz circuits and design of multiband filters.

He is currently a Senior Research Scientist with the National Physical Laboratory (NPL), Teddington, U.K. Prior to joining the NPL, he was a Research Fellow of the University of Birmingham. His current research interests include microwave measurements, microwave filters and multiplexers, and micromachining techniques.

Dr. Shang was a recipient of the Steve Evans-Pughe Prize by the ARMMS RF and Microwave Society, in 2017, and the ARFTG Microwave Measurement Student Fellowship Award, in 2009. He was a co-recipient of the Tatsuo Itoh Award from the IEEE Microwave Theory and Techniques Society, in 2017.

YI WANG (M'09–SM'12) was born in Shandong, China. He received the B.Sc. degree in physics and the M.Sc. degree in condensed matter physics from the University of Science and Technology, Beijing, China, in 1998 and 2001, respectively, and the Ph.D. degree in electronics and electrical engineering from the University of Birmingham, Birmingham, U.K., in 2005.

In 2011, he became a Senior Lecturer and then a Reader with the University of Greenwich. In 2018, he joined the University of Birmingham as a Senior Lecturer. His current research interests include millimeter-wave and terahertz devices for metrology, communications and sensors, micromachining, microwave circuits based on multiport filtering networks, and filter-antenna integration.

MICHAEL J. LANCASTER (SM'04) was born in York, U.K., in 1958. He received the degree in physics and the Ph.D. degree in nonlinear underwater acoustics from Bath University, U.K., in 1980 and 1984, respectively.

After leaving Bath University, he joined the Surface Acoustic Wave (SAW) Group, Department of Engineering Science, Oxford University, as a Research Fellow. He is a Chartered Engineer and a Chartered Physicist. In 1987, he became a Lecturer with the Department of Electronic and Electrical Engineering, University of Birmingham, lecturing in electromagnetic theory and microwave engineering. Shortly after he joined the department, he began the study of the science and applications of high temperature superconductors, working mainly on microwave frequencies. He was promoted as the Head of the Emerging Device Technology Research Center, in 2000, and the Department of Electronics, Electrical and Computer Engineering, University of Birmingham, in 2003. He has published two books and over 170 articles in refereed journals. His research was in the design of new novel SAW devices, including RF filters and filter banks. His current research interests include microwave filters and antennas, and high-frequency properties and applications of a number of novel and diverse materials.

Dr. Lancaster is the Fellow of the IET and the U.K. Institute of Physics. He has served on the IEEE Microwave Theory and Techniques Society International Microwave Symposium Technical Program Committee.

JUN XU was born in Chengdu, China, in 1963. He received the B.S. and M.S. degrees from the University of Electronic Science and Technology of China (UESTC), Chengdu, China, in 1984 and 1990, respectively.

In 1997, he became an Associate Professor with the UESTC, where he is currently the Head of the School of Physics. He was then promoted as a Professor, in 2000. His main research interests include microwave theory and technology, millimeter-wave hybrid integrated technology, millimeter-wave communication and radar radio frequency technology, and the 3-D printing of passive microwave devices.

• • •